Materials Horizons

ROYAL SOCIETY OF CHEMISTRY

COMMUNICATION

View Article Online
View Journal | View Issue

Check for updates

Cite this: *Mater. Horiz.*, 2021, **8**, 2761

Received 26th June 2021,
Accepted 30th July 2021

DOI: 10.1039/d1mh00998b

rsc.li/materials-horizons

Published on 30 2021. Downloaded on 11/23/2025 3:31:55 PM.

A fully hydrophobic ionogel enables highly efficient wearable underwater sensors and communicators†

Junjie Wei,[ab] Yinfei Zheng*[cde] and Tao Chen*[ab]

Underwater sensing has extraordinary significance in ocean exploration (*e.g.*, marine resources development, marine biology research, and marine environment reconnaissance), but the great difference between the marine environment and the land environment seriously prevents current traditional sensors from being applied in underwater sensing. Herein, we reported a fully hydrophobic ionogel with long-term underwater adhesion and stability as a highly efficient wearable underwater sensor that displays an excellent sensing performance, including high sensitivity, rapid responsiveness and superior durability. Of greater significance, the ionogel sensor showed tremendous potential in underwater sensing applications for communication, posture monitoring and marine biological research.

New concepts

In this communication, we demonstrate a new ion-conducting gel with long-term underwater stability for wearable underwater sensors and communicators. Ion-conducting gels are regarded as one of the most promising wearable sensors owing to their great advantages of tunable mechanical properties, stretchability, biocompatibility and multifunctionality. While ion-conducting gels have been studied and applied widely in many fields, their operating environment has been confined to a dry air because their inherent swelling behavior and ion diffusion prevent them from being applied in an aquatic environment. Utilizing a fully hydrophobic structure, this study enables ion-conducting gels to realize a breakthrough in underwater applications, even in a seawater environment. The fully hydrophobic structure endows the ion-conducting gel with superior water-resistance, robust underwater adhesion and outstanding underwater stability. Additionally, the fully hydrophobic ionogel sensor displays an excellent sensing performance in the underwater environment, including high sensitivity (a gauge factor of 1.30), rapid responsiveness (~37 ms) and superior durability (over 5 months). Furthermore, it is confirmed that the ionogel can be applied in the fields of posture monitoring, biological research and underwater communications, performing as a wearable underwater sensor and communicator. Therefore, the fully hydrophobic ionogel is of great significance for broadening the operating environment of ion-conducting gels and accelerating their application in ocean exploration.

Introduction

As a vast and mysterious treasure, the ocean has always attracted people's keen interest for exploration. Wearable underwater sensing is of great significance for ocean exploration because it plays a crucial role in ensuring the exploration safety and improving the exploration efficiency by detecting various signals from both the human and the environment. However, although wearable sensors have attracted considerable attention and gratifying progress has been made for land applications in recent years,[1–6] there is still a tremendous challenge for realizing wearable sensors suitable for underwater sensing applications because of the great difference between the marine environment and the land environment. Due to their great advantages of tunable mechanical properties, stretchability, biocompatibility and multifunctionality,[7–9] ion-conducting gels have been regarded as one of the most promising wearable sensors and have been widely applied in wearable and implantable devices,[10,11] human health monitoring,[12,13] artificial skin,[14,15] soft robots[16,17] and so on. For example, Wu *et al.*[18] have developed a mechanically adaptable hydrogel-based ionic skin sensor that has excellent compliance with curved and dynamic surfaces based on its novel supramolecular mineral structure. In addition, the high-pressure sensitivity of the mineral hydrogel sensor exhibits a great sensing

[a] *Key Laboratory of Marine Materials and Related Technologies, Zhejiang Key Laboratory of Marine Materials and Protective Technologies, Ningbo Institute of Materials Technology and Engineering, Chinese Academy of Sciences, Ningbo 315201, China. E-mail: tao.chen@nimte.ac.cn*

[b] *School of Chemical Sciences, University of Chinese Academy of Sciences, Beijing 100049, China*

[c] *Research Center for Intelligent Sensing, Zhejiang Lab, No. 1818 West Wenyi Road, Yuhang District, Hangzhou 311100, China*

[d] *College of Biomedical Engineering and Instrument Science, Zhejiang University, Hangzhou 310027, China. E-mail: zyfnjupt@zju.edu.cn*

[e] *Key Laboratory for Biomedical Engineering of Ministry of Education Ministry of China, Zhejiang University, Hangzhou 310027, China*

† Electronic supplementary information (ESI) available. See DOI: 10.1039/d1mh00998b

Published on 30 2021. Downloaded on 11/23/2025 3:31:55 PM.

performance for human motion. Unfortunately, due to the swelling capacity of hydrophilic polymer networks[19,20] and the diffusion of conducting ions,[21–23] it is difficult for ion-conducting gel sensors to maintain long-term stability under high humidity conditions, resulting in their unsuitability for application in water and marine environments. Therefore, improving the underwater stability of ion-conducting gels is the key to expanding their environments of application.

In fact, a great deal of effort has been devoted to solving the problem of the swelling of hydrogels, and some useful methods have been developed recently, such as solvent-exchange strategies,[24–26] high-crosslinking densities,[27–29] and hydrophobic modification.[30–32] For example, Deng and Cui *et al.*[30] have demonstrated a class of dynamic hydrogels through the Fe^{3+}-induced self-hydrophobization process, which endows hydrogels with superior underwater stability and adhesion. These specifically designed anti-swelling hydrogels *via* hydrophobic modification or other strategies can undergo long-term immersion in water; however, there is still a huge challenge to restrain the diffusion and loss of conducting ions in the aquatic environment because of a concentration gradient, resulting in the decline and even full loss of conducting and sensing capacities. Recently, Yu and Wu[33] reported an underwater ionogel sensor that utilizes fluorine-rich ionic liquid (IL) monomers and a fluorine-rich IL, and the abundant ion–ion and ion–dipole interactions between the IL (conducting ions) and the poly(ionic liquid) can inhibit the ion diffusion effectively. However, these strong interactions and the high content of the polymer also suppress the migration of ions, which reduce its ionic conductivity and sensing performance. Therefore, it is crucial yet rather challenging to develop a long-term underwater-stable, strongly adhesive and highly conducting gel for wearable underwater sensing applications.

In addition to the concentration gradient, the solvation of ions is also one of the important conditions for the rapid diffusion process. Hence, the problem of diffusion and the loss of conducting ions into the aquatic environment is expected to be solved by suppressing their dissolution process. As is well known, polyacrylates are not only a class of common hydrophobic polymers, but also possess outstanding water-resistance and adhesive characteristics. These properties meet the requirements of designing an anti-swelling network of the adhesive gel. Inspired by this, we designed a fully hydrophobic ionogel through the one-step polymerization of hydrophobic acrylate monomers in a hydrophobic IL solvent. This fully hydrophobic ionogel possesses excellent hydrophobicity, robust adhesion and stable conductivity in the aquatic environment; it also exhibits a superior underwater sensing performance, including high sensitivity, fast responsiveness, and long-term stability. The investigation enabled its profound potential application in ocean exploration.

In this work, the fully hydrophobic ionogel was prepared using a facile method. First, 20 wt% monomer (*tert*-butyl acrylate, *t*-BuA), 0.1 wt% crosslinker (ethylene glycol dimethacrylate, EGDMA) and 0.5 wt% thermal initiator (2,2-azobisisobutyronitrile, AIBN) were dispersed in hydrophobic IL (1-butyl-3-methylimidazolium bis(trifluoromethanesulfonyl) imide, [BMIm]TFSI) to prepare the precursor dispersion. Then, the fully hydrophobic ionogel was formed by thermal-initiation polymerization at 60 °C for 90 min. As shown in Fig. 1a, due to the hydrophobic effect, the abundant hydrophobic tertiary butyl moieties act as a diffusion barrier between the ionogel domains and the water phase, terminating most of the substance transport across the boundaries of the ionogel, playing an important role in suppressing the interfacial diffusion of water molecules and ions. Besides, the intrinsic hydrophobicity of [BMIm]TFSI can prevent ions from diffusing into the water environment. In addition, the hydrogen bond, dipole–dipole and ion–dipole interactions,[33–37] between the polyacrylate polymer network and [BMIm]TFSI not only ensure that the two phases of the ionogel have good compatibility, but also help to lock the IL in the ionogel. Furthermore, owing to these superior properties, the fully hydrophobic ionogel shows great application potential in the field of wearable underwater sensors and communicators (Fig. 1b).

Results and discussion

The fully hydrophobic structure endows the ionogel with an excellent water-resistance ability and long-term underwater stability. As shown in Fig. 2a, four different ionogels synthesized from the hydrophobic/hydrophilic monomers (*t*-BuA; *N*,*N*-dimethylacrylamide, DMAA) and the hydrophobic/hydrophilic ionic liquids ([BMIm]TFSI; 1-butyl-3-methylimidazolium tetrafluoroborate $[BMIm]BF_4$) were characterized using contact angle measurements. Compared with the ionogels consisting of hydrophilic components (DMAA or/and $[BMIm]BF_4$), the fully hydrophobic ionogel has the largest water contact angle (WCA) of 86.9°, indicating that the fully hydrophobic structure is beneficial for improving the water-resistance ability of the ionogel due to the synergistic effect between the hydrophobic components. Besides, these ionogels were soaked in water to study their stability in a real water environment. As shown in Fig. 2b, although the swelling ratio of the fully hydrophobic ionogel rose by 3.8% on the first day, there was no significant change over the next 9 days. This variation tendency is attributed to the transformation of the hydrophobic interface. For the fresh ionogel, the distribution of hydrophobic functional groups (tertiary-butyl) at the interface is relatively sparse, which would fail in preventing water molecular diffusion in the beginning. However, due to the incompatibility between the hydrophobic functional groups and water, the hydrophobic polymers begin to move, and the hydrophobic functional groups self-assemble and form a hydrophobic aggregation through the hydrophobic interactions, just like the self-assembly process of amphiphilic block copolymers in water,[38,39] resulting in a lower surface free energy. The denser hydrophobic interface can suppress the diffusion of molecules more effectively (Fig. 2d). The WCA change of the fully hydrophobic ionogel confirmed this mechanism. As shown in Fig. 2c, the WCA evolved from ~87° to ~120° after soaking in water,

 This journal is © The Royal Society of Chemistry 2021

Published on 30 2021. Downloaded on 11/23/2025 3:31:55 PM.

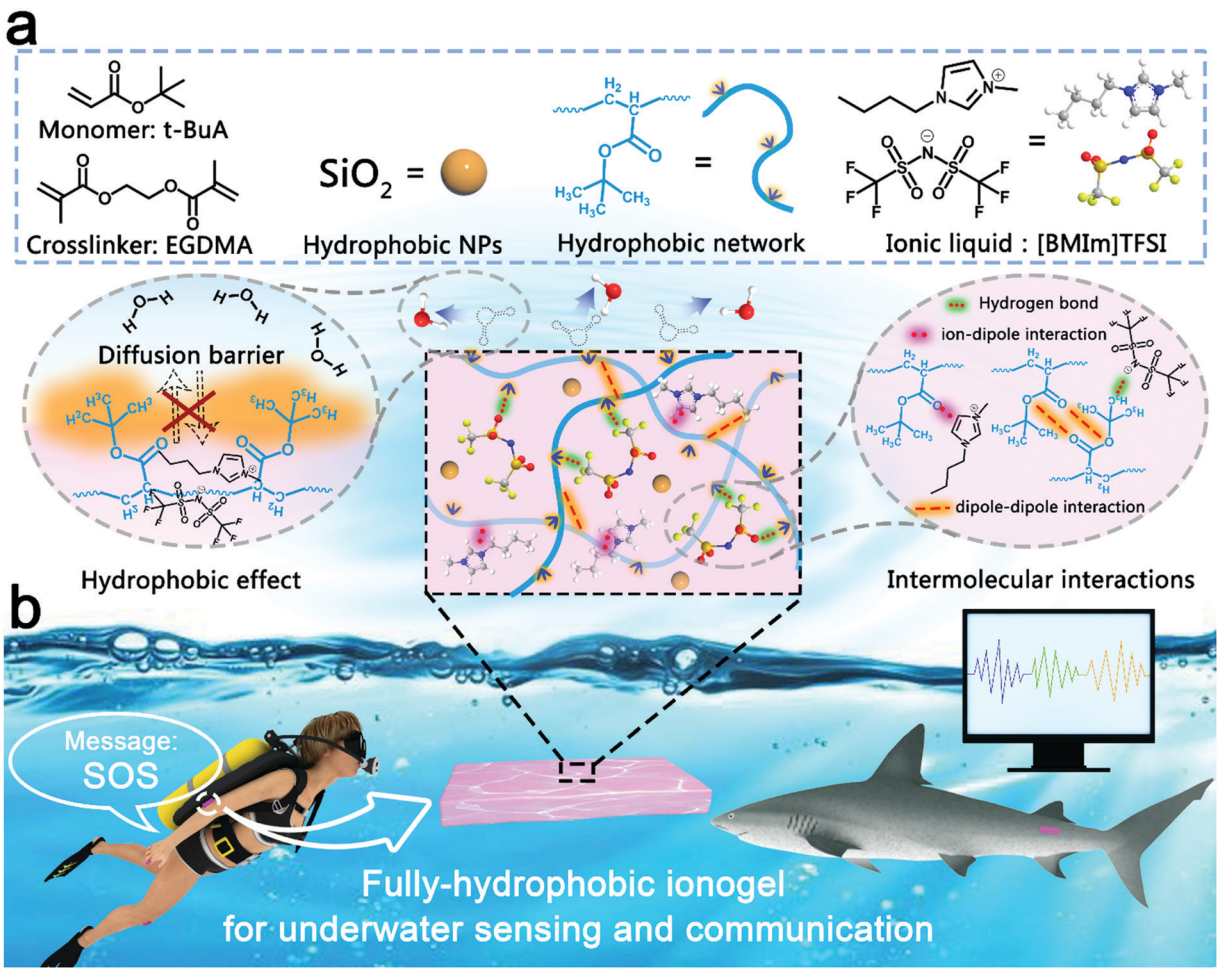

Fig. 1 Schematic of fabricating the fully hydrophobic ionogel for underwater sensors and communicators. (a) Structure of the fully hydrophobic ionogel. (b) Potential applications in underwater sensing and underwater communication.

indicating that the fully hydrophobic ionogel possesses a greater water-resistance ability, which is conducive to long-term underwater stability. By contrast, driven by the osmotic pressure originating from the concentration gradient, the substance (including water molecules and ions) transports freely across the boundaries of the hydrophilic ionogel, resulting in a dramatic change in the swelling ratio (Fig. 2b). The ionic conductivity of the soaking solution was measured to analyze the leakage behavior of the ionic liquid. As shown in Fig. 2e, after soaking for 10 days, the soaking solution of the fully hydrophobic ionogel had the lowest ionic conductivity of 0.28 mS cm^{-1}, confirming that the fully hydrophobic structure can suppress the diffusion and leakage of conducting ions effectively. While the ionic conductivity of the fully hydrophobic ionogel increased slightly from 1.6 mS cm^{-1} to 2.5 mS cm^{-1} early in the period due to the assistance of water molecules, the value remained stable during the subsequent soaking process (Fig. 2f). All the results confirmed that the pre-soaking-treated fully hydrophobic ionogel can maintain its long-term stability in the water environment. In order to improve its stability, the ionogel that had been soaked for 3 days was chosen as the study object for the subsequent experiments.

The mechanical properties are one of the essential parameters for a strain sensor. In order to maintain the structural integrity and sensing performance of the ionogel sensor under large deformations, a certain mass of hydrophobic SiO_2 nanoparticles (NPs) was added into the fully hydrophobic ionogel as a nanofiller to adjust the mechanical properties. As shown in Fig. 2g and h, the mechanical properties of the ionogel were measured *via* the tensile test. The breaking strain of the ionogel gradually increased from 363.3% to 1145.7% as the SiO_2 content was increased from 0 to 3.0 wt% because the reversible hydrophobic interactions between the hydrophobic network and the hydrophobic SiO_2 NPs can dissipate the energy effectively. Interestingly, the breaking stress and the modulus of the ionogel achieve the maximum values of 115.6 kPa and 14.6 kPa, respectively, when the SiO_2 content is 2 wt%, which may be because of too high a SiO_2 content causing an uneven dispersion of SiO_2 within the ionogel. Taking into account both the elongation and the strength, the ionogel with 2 wt% SiO_2 exhibits a satisfactory strain range and mechanical safety. Besides, the ionogel with 2 wt% SiO_2 shows good fatigue resistance properties in the cyclic tensile tests (Fig. S1, ESI†). Notably, after soaking for 3 days, the 2 wt% SiO_2-based fully

Published on 30 2021. Downloaded on 11/23/2025 3:31:55 PM.

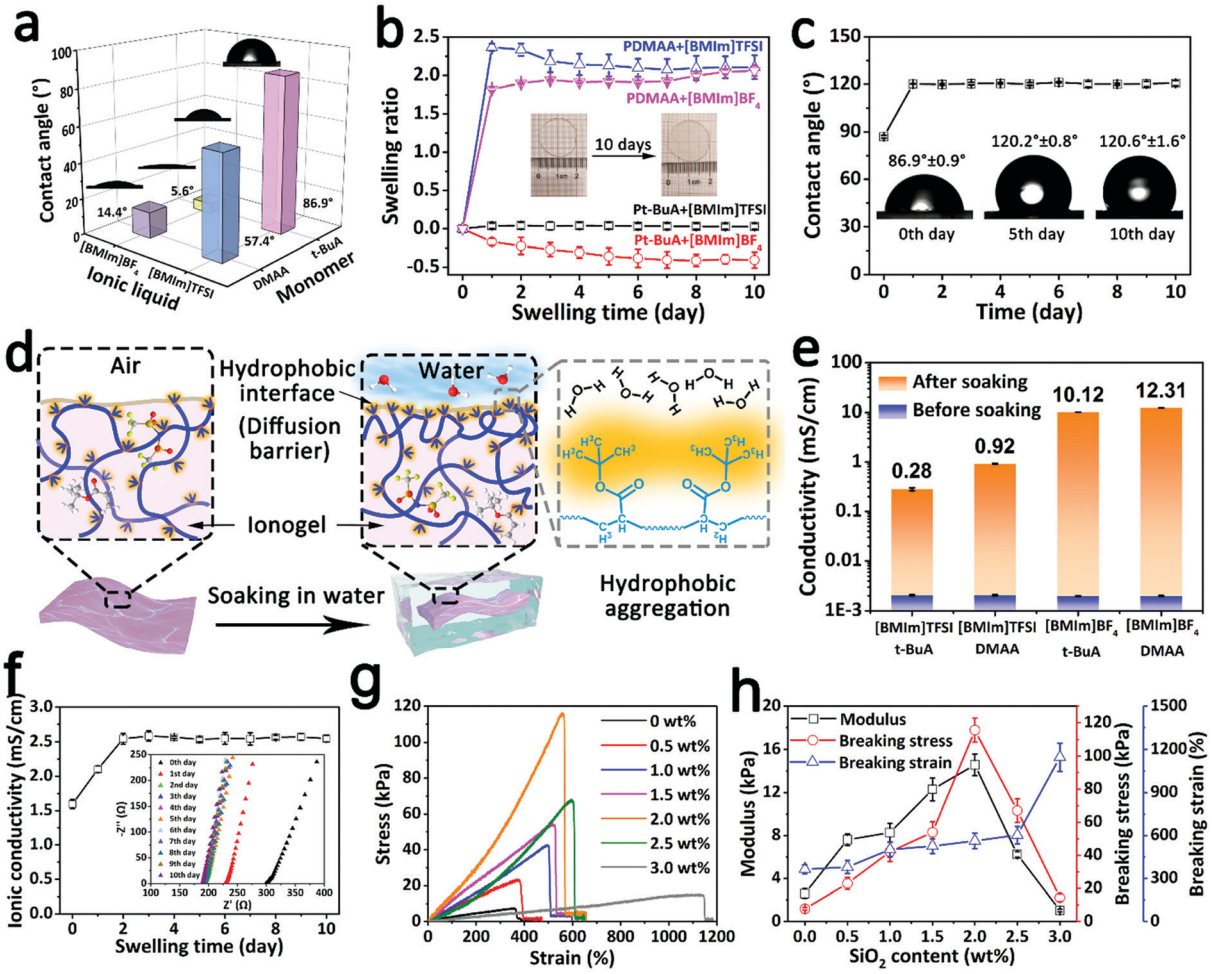

Fig. 2 Hydrophobic and mechanical performances of the fully hydrophobic ionogel. (a) WCA of various ionogels prepared using different monomers and ILs. (b) Swelling behavior of various ionogels during the soaking process. Inset: Digital images of the fully hydrophobic ionogel before and after soaking treatment. (c) WCA change of the fully hydrophobic ionogel during the soaking process. (d) Hydrophobic aggregation schematic diagram of polymers after soaking treatment. (e) Ionic conductivity comparison of the soaking solution for various ionogels, before and after soaking for 10 days. (f) Ionic conductivity change of the Pt-BuA-[BMIm]TFSI ionogel during the soaking process. (g) Tensile curves of the fully hydrophobic ionogel with different mass ratios of SiO_2 NPs. (h) Mechanical properties of the fully hydrophobic ionogel with different mass ratios of SiO_2 NPs.

hydrophobic ionogel exhibited a high and stable ionic conductivity of 2.6 mS cm^{-1} (Fig. S2, ESI†), providing a reliable basis for long-term stability and a brilliant sensing performance. Hence, the 2 wt% SiO_2-based fully hydrophobic ionogel was selected for subsequent studies.

The fully hydrophobic ionogel demonstrated remarkable adhesive properties. As shown in Fig. 3a, the fully hydrophobic ionogel can robustly adhere to diverse materials (including glass, plastic, silicone, textile, steel and copper) and hold the substrate weight in both air and underwater environments. 90° peeling-off tests were carried out to further evaluate the ionogel–substrate adhesion. As shown in Fig. 3b, in the underwater environment, the peeling adhesive strengths of the ionogel for glass, plastic, silicone, textile, steel, copper, nitrile rubber and skin were about 373, 707, 702, 320, 179, 604, 178, and 200 N m^{-1}, respectively. When compared with the value in air (Fig. 3c and Fig. S3, ESI†), there is no significant decline in the adhesive strength. Furthermore, the ionogel exhibited good long-term adhesion stability and stable repeated adhesion ability in underwater adhesion measurements (Fig. S4, ESI†). The robust ionogel–substrate adhesion could be explained by the synergy of chemical bonding and energy dissipation during peeling. As illustrated in Fig. 3d, there are abundant and strong dipole–dipole interactions, ion–dipole interactions, electrostatic interactions and van der Waals interactions between the ionogel and the substrate. These reversible interactions not only bond the ionogel and the substrate powerfully when the two come into contact, but they also dissipate energy effectively when the two come apart. More importantly, the hydrophobic effect can destroy the hydrated layer of the underwater adhesive and enhance the adhesion interaction in water. As a demonstration, the fully hydrophobic ionogel can act as a sealing tape to mend a hole and stop water leakage immediately (Fig. 3e and Video S1, ESI†). Strong underwater adhesion contributes to the practical use of ionogel sensors and accurate acquisition and output of sensing signals.

 This journal is © The Royal Society of Chemistry 2021

Published on 30 2021. Downloaded on 11/23/2025 3:31:55 PM.

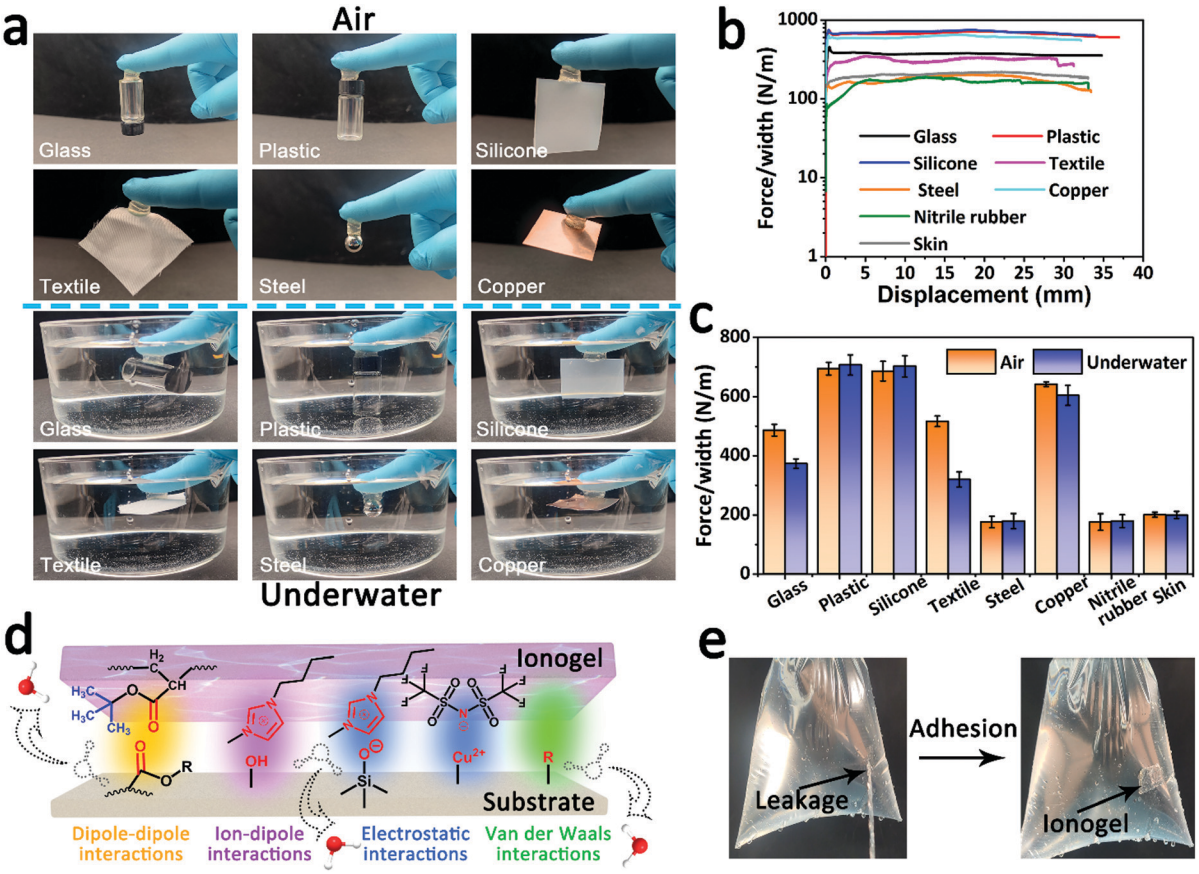

Fig. 3 Adhesive performance of the fully hydrophobic ionogel. (a) Adhesive behavior of the ionogel with various substrates in air/under water. (b) Peeling curves of the ionogel with various substrates under water. (c) Adhesion strength of the ionogel with various substrates in air/under water. (d) Adhesion mechanisms between the ionogel and the substrate. (e) Digital images of mending a hole.

Owing to its satisfactory mechanical properties, high ionic conductivity, robust adhesive ability and outstanding underwater stability, the fully hydrophobic ionogel can be used as an underwater strain sensor. As shown in Fig. 4a, the fully hydrophobic ionogel sensor exhibited high sensitivity and a broad sensing range in the underwater environment. The gauge factor (GF) was calculated to quantify the sensitivity of the ionogel sensor. The relative resistance of the ionogel sensor linearly increased as the strain was increased to 400%, and the ionogel presented a high GF in the tensile strain process. For example, the GF reached a maximum value of 1.30 in the strain range of 0–100%, which is a competitive and even superior performance compared with other previously reported ionogel strain sensors for air applications.[14,34,40,41] This high sensitivity and wide linearity of strain is attributed to its good mechanical properties, high ionic conductivity and the presence of SiO_2 NPs. As shown in Fig. S5a (ESI†), when the ionogel is stretched, the SiO_2 NPs will aggregate in the unit cross-section of the ionogel, which greatly impedes the migration of ions and sharply increases the resistance. The lower GF value of the 0 wt% SiO_2-based ionogel sensor also confirmed this hypothesis (Fig. S5b, ESI†).

Due to its high sensitivity and recoverability, the relative resistance of the ionogel sensor showed reversible and stable changes over a wide strain range, including low strains (5–30%) (Fig. 4b) and high strains (50–400%) (Fig. S6, ESI†), which suggested that the ionogel sensor shows perfect reliability for detecting various strains. Moreover, the ionogel sensor exhibited good frequency responsiveness, which plays a vital role in wearable applications. As shown in Fig. 4c, the ionogel sensor can continuously, rapidly and accurately monitor the different strain frequencies from 0.1 to 1.5 Hz. The response speed is another key parameter for evaluating the sensing performance. When the ionogel sensor was stretched and allowed to recover quickly, the response times for stretching and recovering processes were 37 ms and 98 ms (Fig. 4d), respectively, even faster than that of human skin (~100 ms).[42] This fast signal responsiveness endows the ionogel sensor with real-time monitoring ability. As shown in Fig. 4e, there is negligible hysteresis between the relative resistance and the tensile strain, indicating that the output response signal can synchronize with the input strain signal, thereby realizing real-time detection and output of the motion signal. In addition, although the temperature change of water can greatly affect the ionic conductivity of the ionogel, its relative resistance is still stable, and the ionogel sensor can operate with steady sensitivity over a wide water temperature range of 0–80 °C (Fig. 4f). This temperature insensitivity can significantly decrease the effect of the

Published on 30 2021. Downloaded on 11/23/2025 3:31:55 PM.

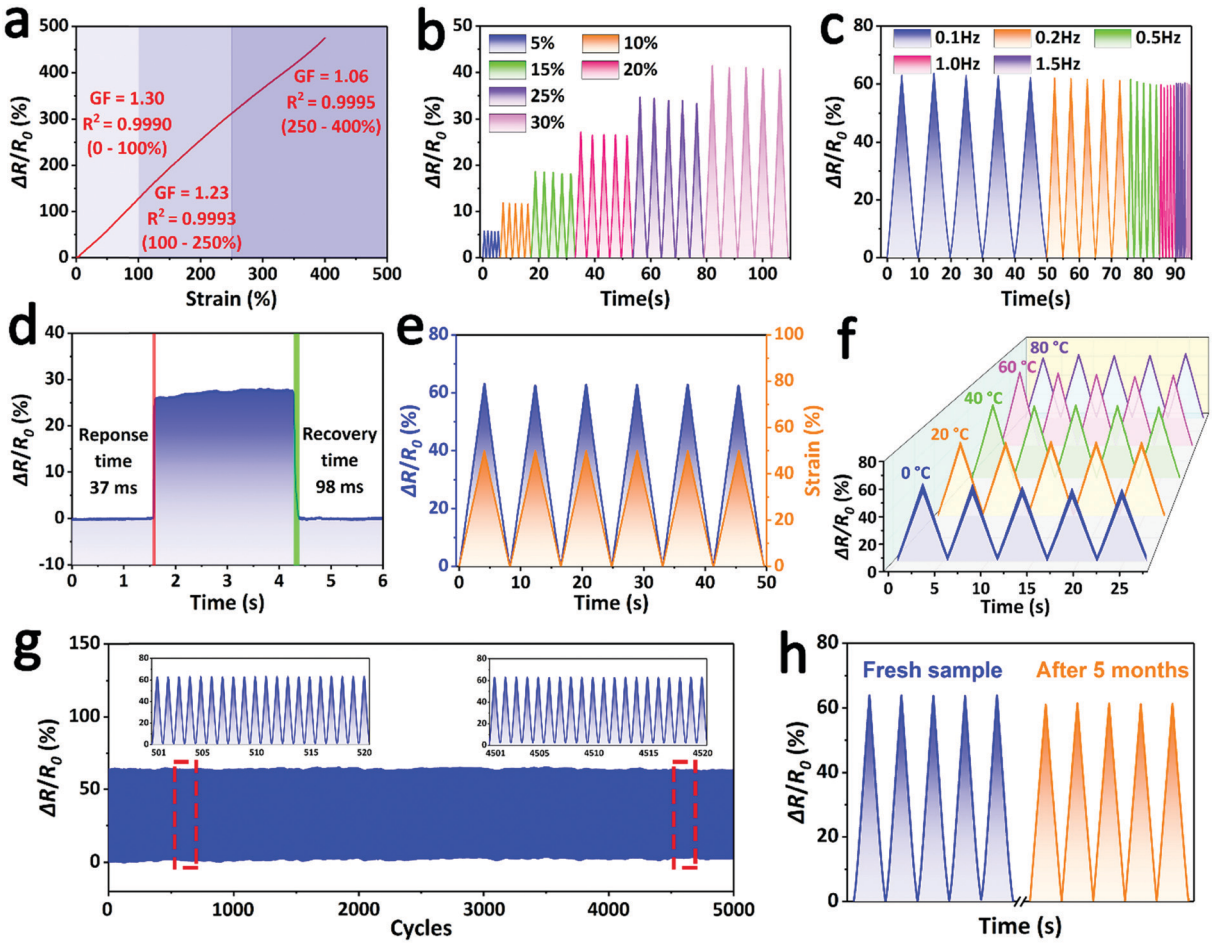

Fig. 4 Underwater sensing performance of the fully hydrophobic ionogel sensor. (a) Gauge factor of the ionogel sensor with segmented strain regions. (b) Relative resistance variation of the ionogel sensor under small strains of 5–30%. (c) Relative resistance variation of the ionogel sensor under different stretching frequencies at 50% strain. (d) Response time of the ionogel sensor. (e) Tensile strain–time curve and the relative resistance–time curve. (f) Relative resistance variation of the ionogel sensor under 50% strain at different water temperatures. (g) Cycling stability of the ionogel sensor for 5000 cycles at 50% strain. Inset: Enlarged signals of the relative resistance variation in the 501st–520th and 4501st–4520th cycles. (h) Relative resistance comparison of the ionogel sensor before and after soaking for 5 months.

temperature change and greatly improve the environmental adaptability of the sensor. Furthermore, the ionogel sensor demonstrated prominent fatigue resistance to strain sensing. As shown in Fig. 4g, after undergoing 5000 loading–unloading cycles, the relative resistance intensity of the ionogel sensor declined negligibly due to its stable mechanical properties and electrical properties. This sensing stability confirms the durability and usability of the ionogel sensor in the underwater environment. More significantly, the ionogel still presented a stable and consistent relative resistance even after 5 months of soaking treatment, although a slight intensity decay of $\sim$4.7% was found because of the unavoidable degradation (Fig. 4h). This amazing underwater stability, derived from full hydrophobicity, is expected to greatly extend the lifespan of the ionogel sensor in practical applications.

This ionogel sensor, which features an excellent performance, including robust adhesion, high sensitivity, a fast response speed and long-term sensing stability, has great potential for multifunctional underwater applications. As shown in Fig. 5a, the ionogel sensor was fixed on a finger to monitor its bending motion under water. When the straight finger was gradually bent from 0° to 90°, the output signal intensity of the relative resistance steadily increased synchronously due to the stretching of the skin. By contrast, the relative resistance gradually decreased when the finger was returned to the straight state. Additionally, the change tendency of the relative resistance can also be used to distinguish between the bending and restoring processes of the finger. For instance, the increasing relative resistance implies that the finger is bending, and the decreasing signal implies that the bent finger is being restored.

Furthermore, the ionogel sensor attached to a finger can be applied as an efficient piece of underwater communication equipment (underwater communicator) for divers by monitoring and outputting the finger motion signals. It is universally acknowledged that diving is one of the most important ways to investigate the submarine resources, but it is inefficient and dangerous for divers where there is the lack of an effective

 This journal is © The Royal Society of Chemistry 2021

Published on 30 2021. Downloaded on 11/23/2025 3:31:55 PM.

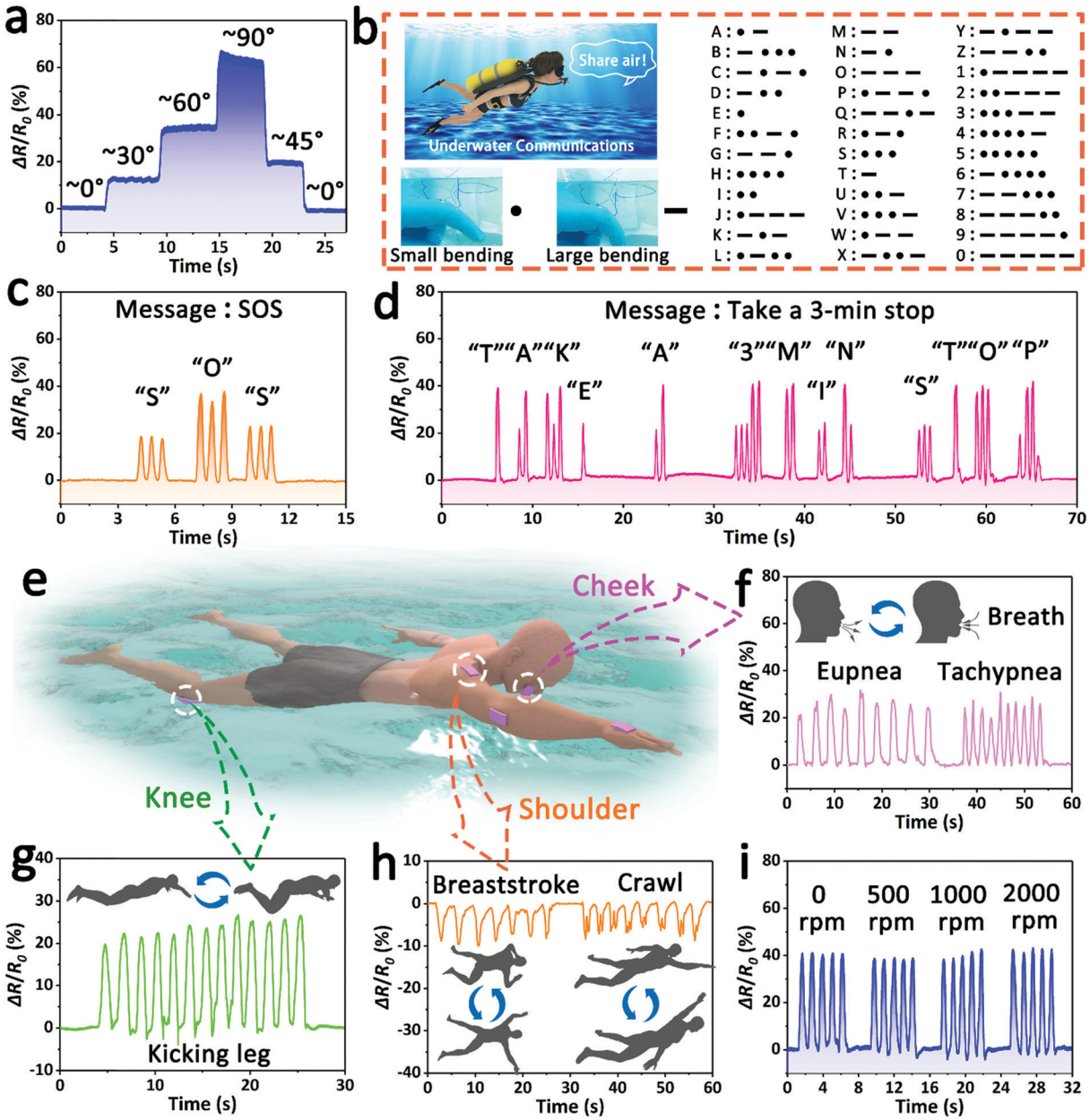

Fig. 5 Applications of the fully hydrophobic ionogel sensor for underwater communication and underwater human motion monitoring. (a) Relative resistance variation of the ionogel sensor under different bending angles of the finger. (b) Schematic diagram of the underwater communication mechanism based on the Morse code. (c and d) Sending the message of "SOS" (c) and "take a 3 min stop" (d) by bending the finger regularly under water. (e) Schematic diagram of the ionogel sensor monitoring human motion during swimming. (f–h) Relative resistance variation of the ionogel sensor when monitoring the breath (f), kicking the leg (g) and the swimming stroke (h) during swimming by fixing the ionogel sensor on the cheek, knee and shoulder, respectively. (i) Relative resistance variation of the ionogel sensor in rotated water with a revolving speed of 0–2000 rpm.

underwater communication method. In this work, by using the coding principle of Morse code, that is the combination of "dots" and "dashes", and matching the finger bending status to "dots" and "dashes", we established a new underwater communication mechanism—the small bending state (~40°) represents the "dots", and the large bending state (~70°) represents the "dashes" (Fig. 5b). Thus, through the continuous combination of finger bending episodes, a series of useful messages can be easily sent in the underwater environment. As a validation, some simple demonstrations were carried out. During a dive, the diver wearing an ionogel communicator can send a short message of "SOS" by rhythmically bending their finger to call for help in the case of danger (Fig. 5c), and send the message of "OK" to their partner when they arrive safely at the designated location (Fig. S7a, ESI†). Similarly, when the diver is short of oxygen, they can turn to their partner for oxygen by sending "share air" (Fig. S7b, ESI†). Before surfacing, the diver can remind their partner to make a safe stop to prevent decompression sickness by sending a long message of "take a 3 min stop" (Fig. 5d). As demonstrated above, the

Published on 30 2021. Downloaded on 11/23/2025 3:31:55 PM.

ionogel sensor is expected to promote underwater exploration by providing a practical means of underwater communication.

In addition to the finger, the ionogel can be attached to other parts of the human body as wearable sensors to monitor human sports, such as swimming (Fig. 5e). As shown in Fig. 5f, the ionogel sensor was adhered to the cheek of a volunteer to monitor and record the breathing process during a simulated swim. The ionogel sensor can accurately perceive and differentiate the intensity and frequency of the breath, meaning that the fatigue level of the swimmer can be roughly evaluated, and reasonable suggestions can be provided in time. In addition, leg and arm movements can be continuously detected in real time by fixing the ionogel sensor to the knee and elbow (Fig. 5g and Fig. S8a, ESI†). More interestingly, owing to its high sensitivity, the ionogel sensor can be used to distinguish swimming strokes (breaststroke and crawl) by monitoring the motion of the shoulder (Fig. 5h). When the ionogel was adhered to the back of the hand, it can also be used to detect the action of striking water during the swimming process (Fig. S8b, ESI†). It is worth noting that the water disturbance caused by sports has no significant effect on the sensing signal. The ionogel sensor attached to the finger was soaked in rotated water to study its sensing stability. As shown in Fig. 5i, the sensing signal of the finger motion remained stable all the time, although the revolving speed of water increased from 0 rpm to 2000 rpm. The good anti-disturbance capacity ensures the accuracy and reliability of the underwater sensing signal. These results suggest that the ionogel sensor has great

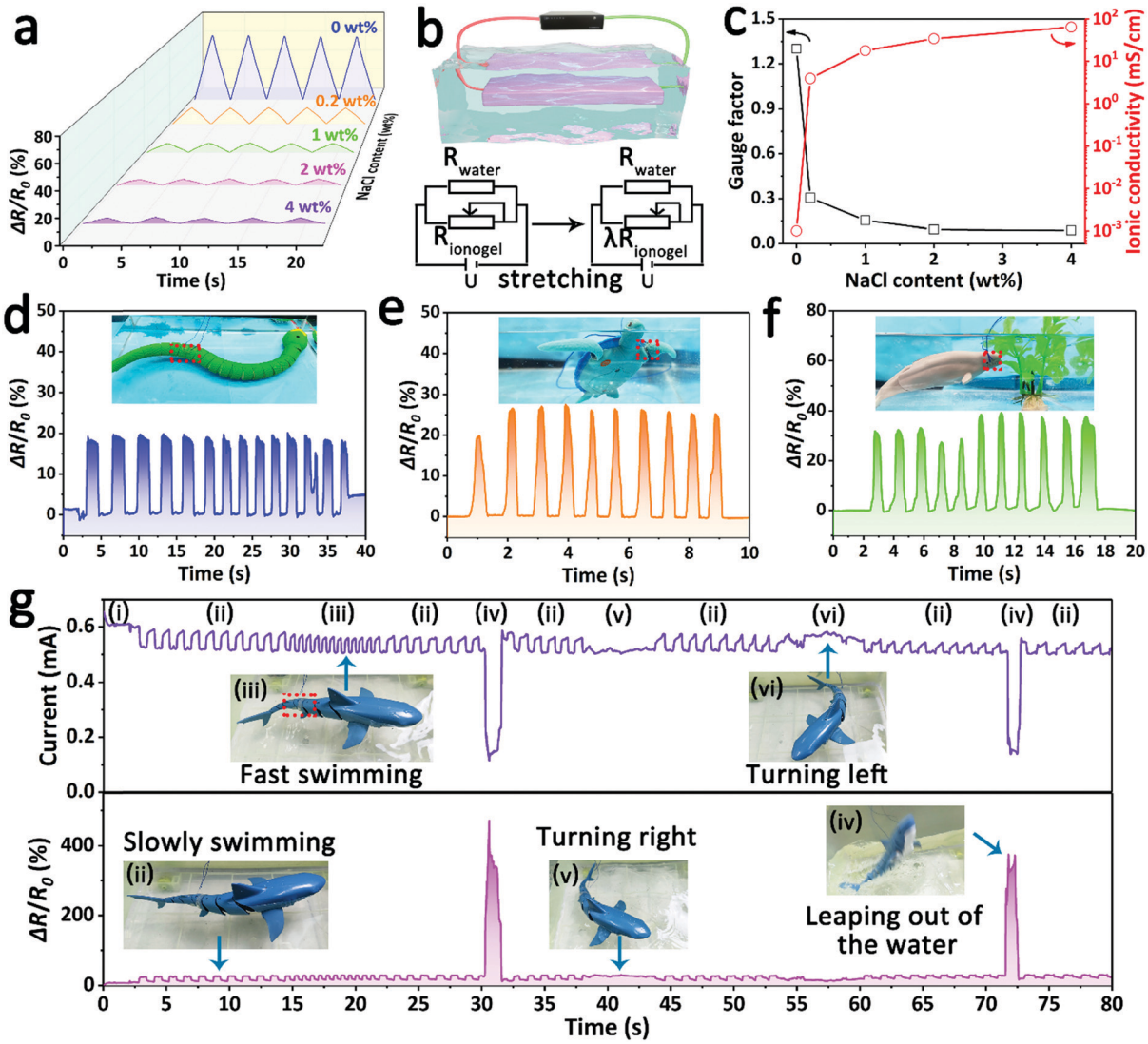

Fig. 6 Applications of the fully hydrophobic ionogel sensor for underwater biological monitoring. (a) Relative resistance comparison of the ionogel sensor in salt solution with different NaCl contents. (b) Analog circuit of the ionogel sensor in conductive soaking solution. (c) Relationship between the gauge factor of the ionogel sensor and the ionic conductivity of the soaking solution. (d–f) Relative resistance variation of the ionogel sensor monitoring the swimming of an aquatic snake model (d), the paddling of a turtle model (e) and the eating of a dolphin model (f) in the simulated seawater. (g) Real-time sensing signal of the ionogel sensor monitoring shark model's swimming states, including resting (i), swimming slowly (ii), fast swimming (iii), leaping out of the water (iv), turning right and (v) turning left (vi).

 This journal is © The Royal Society of Chemistry 2021

Published on 30 2021. Downloaded on 11/23/2025 3:31:55 PM.

potential in security warning, motion monitoring and posture correction for underwater sports.

Different from the simulated water environment mentioned above, some natural waters (*e.g.*, salt lakes and oceans) contain a certain concentration of salts. Thus, the ionogel was soaked in a salt solution with a certain concentration of NaCl to study its availability in such a real-water area. As shown in Fig. 6a, although the relative resistance rapidly decreased as the NaCl content was increased from 0 wt% to 4 wt%, the detection signal is still accurate and discernible even at the high NaCl content of 4 wt%. This phenomenon of decreased sensing intensity is attributed to the increased ionic conductivity of the solution. In this system, the conductive NaCl solution, acting as a fixed resistor, is in parallel with the ionogel sensor in the circuit (Fig. 6b). Therefore, the resistance change in the tensile process will be mainly affected by the resistance of the NaCl solution. According to the simplified derived formula for the GF value (eqn (S7), ESI†), the GF value decreased with the decreasing solution resistance. This conclusion is in good agreement with the experimental results that there is a negative correlation between the GF value and the conductivity of the NaCl solution (Fig. 6c). Besides, the sensing feasibility of the ionogel sensor in highly conductive solutions (64.2 mS cm^{-1}, 4 wt% NaCl solution) implies that it can be used in most natural waters due to the inherent high ionic conductivity of the ionogel sensor. As a demonstration, the ionogel sensor was attached to some underwater animal models to detect their motions in simulated seawater (3.5 wt% NaCl solution). As shown in Fig. 6d–f, the sensing signals of various motions, including the swimming of an aquatic snake model, the paddling of a turtle model and the eating of a dolphin model, were clear and distinguishable. Furthermore, the ionogel sensor can accurately monitor various continuous and complex movements of underwater animals in real time if it is fixed on a suitable part. A shark model with a shakable tail was chosen for the demonstration, and the ionogel sensor was attached to the right side of the shark model's tail. As shown in Fig. 6g and Video S2 (ESI†), the electrical signal of the tail's motions can be continuously captured during the swimming process. In addition, by distinguishing the intensity and frequency of the signal, the shark's various swimming modes can be estimated, including rest, swimming slowly, fast swimming, leaping out of the water, turning right and turning left. For example, the swimming speed can be evaluated by the signal frequency because the speed is determined by the swing frequency of the tail. When the shark is turning right or left, the tail will bend to the left or right for a longer time, and the ionogel sensor is correspondingly in a state of stretch or compression. Thus, the direction of the turn can be judged by the signal intensity and duration period. The big difference in conductivity between the simulated seawater and air can lead to a drastic change in the signal intensity, which provides a reliable criterion of whether or not the shark is out of the water. The above demonstrations fully demonstrate the great potential of ionogel sensors in studying and tracking the living habits of marine organisms. Although the risk of liquid leakage is low at high pressure due to the abundant and strong interactions between polymer networks and ionic liquids (Fig. S9, ESI†), the possible ecological safety of this ionogel needs to be further studied, especially in the deep-sea environment.

Conclusions

In summary, a fully hydrophobic ion-conducting ionogel with excellent long-term underwater stability was successfully developed by the simple one-step polymerization of hydrophobic monomers in a hydrophobic IL solvent. By establishing the diffusion barrier, the fully hydrophobic structure not only endowed the ionogel with outstanding water resistance, but also suppressed the diffusion of ions effectively, leading to a stable ionic conductivity under the water. Besides, the great hydrophobic properties also enhanced the adhesion of the ionogel in the underwater environment by destroying the hydration layer. Furthermore, due to its satisfactory conductivity, good mechanical properties and prominent long-term underwater stability, the ionogel exhibited high sensitivity, a wide strain range, rapid responsiveness and superior durability when it performed as an underwater strain sensor. Moreover, the ionogel sensor can accurately detect the body motions of human and aquatic life for posture monitoring and biological research in the complex underwater environment, even in simulated seawater. More significantly, performing as the underwater communicator, the ionogel sensor can be used to efficiently transmit information through monitoring the regular bending of a finger and utilizing the principle of Morse code. As a promising candidate for a water-resistant ion-conducting gel, the fully hydrophobic ionogel exhibits excellent underwater sensing and communication performance for potential ocean applications and provides a simple and effective route for next-generation wearable underwater sensors and communicators.

Author contributions

J. W. and T. C. conceived the project and designed the experiments. Y. Z. and T. C. guided the project. J. W. performed the experiment and analyzed the data. All the authors discussed and reviewed the manuscript.

Conflicts of interest

The authors declare no competing financial interest.

Acknowledgements

This work was supported by the National Natural Science Foundation of China (51773215), National Key R&D Program of China, Ministry of Science and Technology of China (2018YFC0114900), the China Postdoctoral Science Foundation (2021M690157), the Key Research Program of Frontier Science, Chinese Academy of Sciences (QYZDB-SSW-SLH036),

Published on 30 2021. Downloaded on 11/23/2025 3:31:55 PM.

the Sino-German Mobility Program (M-0424), and the K. C. Wong Education Foundation (GJTD-2019-13).

Notes and references

1 S. Lee, S. Franklin, F. A. Hassani, T. Yokota, O. G. Nayeem, Y. Wang, R. Leib, G. Cheng, D. W. Franklin and T. Someya, *Science*, 2020, **370**, 966–970.
2 I. You, D. G. Mackanic, N. Matsuhisa, J. Kang, J. Kwon, L. Beker, J. Mun, W. Suh, T. Y. Kim, J. B. H. Tok, Z. N. Bao and U. Jeong, *Science*, 2020, **370**, 961–965.
3 O. A. Araromi, M. A. Graule, K. L. Dorsey, S. Castellanos, J. R. Foster, W. H. Hsu, A. E. Passy, J. J. Vlassak, J. C. Weaver, C. J. Walsh and R. J. Wood, *Nature*, 2020, **587**, 219–224.
4 Y. Wang, H. T. Wu, L. Xu, H. N. Zhang, Y. Yang and Z. L. Wang, *Sci. Adv.*, 2020, **6**, eabb9083.
5 H. D. Liu, H. J. Zhang, W. Q. Han, H. J. Lin, R. Z. Li, J. X. Zhu and W. Huang, *Adv. Mater.*, 2021, **33**, 2004782.
6 Y. Z. Ling, T. C. An, L. W. Yap, B. W. Zhu, S. Gong and W. L. Cheng, *Adv. Mater.*, 2020, **32**, 1904664.
7 C. H. Yang and Z. G. Suo, *Nat. Rev. Mater.*, 2018, **3**, 125–142.
8 H. Yuk, B. Y. Lu and X. H. Zhao, *Chem. Soc. Rev.*, 2019, **48**, 1642–1667.
9 Z. W. Wang, Y. Cong and J. Fu, *J. Mater. Chem. B*, 2020, **8**, 3437–3459.
10 Y. Gao, S. Gu, F. Jia and G. H. Gao, *J. Mater. Chem. A*, 2020, **8**, 24175–24183.
11 X. J. Pei, H. Zhang, Y. Zhou, L. J. Zhou and J. Fu, *Mater. Horiz.*, 2020, **7**, 1872–1882.
12 X. Y. Liu, C. Steiger, S. T. Lin, G. A. Parada, J. Liu, H. F. Chan, H. Yuk, N. V. Phan, J. Collins, S. Tamang, G. Traverso and X. H. Zhao, *Nat. Commun.*, 2019, **10**, 493.
13 M. Wu, J. S. Chen, Y. H. Ma, B. Yan, M. F. Pan, Q. Y. Peng, W. D. Wang, L. B. Han, J. F. Liu and H. B. Zeng, *J. Mater. Chem. A*, 2020, **8**, 24718–24733.
14 T. Q. Li, Y. T. Wang, S. H. Li, X. K. Liu and J. Q. Sun, *Adv. Mater.*, 2020, **32**, 2002706.
15 J. Wen, J. Tang, H. M. Ning, N. Hu, Y. Y. Zhu, Y. K. Gong, C. H. Xu, Q. N. Zhao, X. P. Jiang, X. L. Hu, L. Lei, D. Wu and T. Huang, *Adv. Funct. Mater.*, 2021, **31**, 2011176.
16 R. A. John, N. Tiwari, M. I. Bin Patdillah, M. R. Kulkarni, N. Tiwari, J. Basu, S. K. Bose, Ankit, C. J. Yu, A. Nirmal, S. K. Vishwanath, C. Bartolozzi, A. Basu and N. Mathews, *Nat. Commun.*, 2020, **11**, 4030.
17 J. Yeom, A. Choe, S. Lim, Y. Lee, S. Na and H. Ko, *Sci. Adv.*, 2020, **6**, eaba5785.
18 Z. Y. Lei, Q. K. Wang, S. T. Sun, W. C. Zhu and P. Y. Wu, *Adv. Mater.*, 2017, **29**, 1700321.
19 H. C. Yu, S. Y. Zheng, L. T. Fang, Z. M. Ying, M. Du, J. Wang, K. F. Ren, Z. L. Wu and Q. Zheng, *Adv. Mater.*, 2020, **32**, 2005171.
20 F. Wu, Y. Pang and J. Y. Liu, *Nat. Commun.*, 2020, **11**, 4502.
21 Z. Zhang, L. He, C. C. Zhu, Y. C. Qian, L. P. Wen and L. Jiang, *Nat. Commun.*, 2020, **11**, 875.
22 J. J. Wei and Q. G. Wang, *Small Methods*, 2019, **3**, 1900558.
23 X. Yao, L. Chen, J. Ju, C. H. Li, Y. Tian, L. Jiang and M. J. Liu, *Adv. Mater.*, 2016, **28**, 7383–7389.
24 L. J. Xu, S. Gao, Q. R. Guo, C. Wang, Y. Qiao and D. Qiu, *Adv. Mater.*, 2020, **32**, 2004579.
25 X. Liu, Q. Zhang and G. H. Gao, *ACS Nano*, 2020, **14**, 13709–13717.
26 X. Liu, Q. Zhang, L. J. Duan and G. H. Gao, *ACS Appl. Mater. Interfaces*, 2019, **11**, 6644–6651.
27 Z. Y. Xu, C. C. Fan, Q. Zhang, Y. Liu, C. Y. Cui, B. Liu, T. L. Wu, X. P. Zhang and W. G. Liu, *Adv. Funct. Mater.*, 2021, **31**, 2100462.
28 H. L. Fan, J. H. Wang and Z. X. Jin, *Macromolecules*, 2018, **51**, 1696–1705.
29 H. L. Fan, J. H. Wang and J. P. Gong, *Adv. Funct. Mater.*, 2021, **31**, 2009334.
30 L. Han, M. H. Wang, L. O. Prieto-Lopez, X. Deng and J. X. Cui, *Adv. Funct. Mater.*, 2020, **30**, 1907064.
31 Y. L. Wang, X. Yao, S. W. Wu, Q. Y. Li, J. Y. Lv, J. J. Wang and L. Jiang, *Adv. Mater.*, 2017, **29**, 1700865.
32 F. Mo, G. Liang, D. Wang, Z. Tang, H. Li and C. Zhi, *EcoMat*, 2019, **1**, e12008.
33 Z. C. Yu and P. Y. Wu, *Adv. Mater.*, 2021, **33**, 2008479.
34 Z. Q. Cao, H. L. Liu and L. Jiang, *Mater. Horiz.*, 2020, **7**, 912–918.
35 Y. Cao, H. Wu, S. I. Allec, B. M. Wong, D. Nguyen and C. Wang, *Adv. Mater.*, 2018, **30**, 1804602.
36 Z. C. Yu and P. Y. Wu, *Mater. Horiz.*, 2021, **8**, 2057–2064.
37 Y. Cao, Y. J. Tan, S. Li, W. W. Lee, H. Guo, Y. Cai, C. Wang and B. C.-K. Tee, *Nat. Electron.*, 2019, **2**, 75–82.
38 T. Zhou, J. Zhu, L. Gong, L. Nong and J. Liu, *J. Am. Chem. Soc.*, 2019, **141**, 2852–2856.
39 W. Wen, T. Huang, S. Guan, Y. Zhao and A. Chen, *Macromolecules*, 2019, **52**, 2956–2964.
40 Y. S. Xie, R. Xie, H. C. Yang, Z. W. Chen, J. W. Hou, C. R. Lopez-Barron, N. J. Wagner and K. Z. Gao, *ACS Appl. Mater. Interfaces*, 2018, **10**, 32435–32443.
41 M. R. Crump, A. T. Gong, D. Chai, S. L. Bidinger, F. J. Pavinatto, T. E. Reihsen, R. M. Sweet and J. D. MacKenzie, *Nanotechnology*, 2019, **30**, 364002.
42 R. S. Johansson and J. R. Flanagan, *Nat. Rev. Neurosci.*, 2009, **10**, 345–359.

 This journal is © The Royal Society of Chemistry 2021